Adsorption of oxygen on Pt3Sn studied by scanning tunneling microscopy and x-ray photoelectron diffraction

Adsorption of oxygen on $Pt_3Sn(111)$ studied by scanning tunneling microscopy and x-ray photoelectron diffraction

M. Hoheisel* and S. Speller
Research Institute for Materials, University of Nijmegen, 6525 ED Nijmegen, The Netherlands

W. Heiland
Fachbereich Physik, Universität Osnabrück, 49069 Osnabrück, Germany

A. Atrei
Dipartimento di Scienze e Tecnologie Chimiche, Università di Siena, I-53100 Siena, Italy

U. Bardi and G. Rovida
Dipartimento di Chimica, Università di Firenze, I-50121 Firenze, Italy
(Received 11 April 2002; published 25 October 2002)

The adsorption of oxygen on the (111) surface of the Pt_3Sn alloy was studied by means of scanning tunneling microscopy (STM) and x-ray photoelectron diffraction (XPD). As Auger electron spectroscopy, low-energy ion scattering, and x-ray photoelectron spectroscopy indicate, upon oxygen exposure (range 10000 L, with the sample at circa 770 K) Sn segregates to the surface and forms a two-dimensional tin-oxygen layer. In the x-ray photoemission spectra no pronounced chemical shift is visible that would indicate a thicker tin oxide layer. After exposure to 10000 L O_2 at 770 K low-energy electron diffraction shows a streaky 2×2 pattern with additional spots. Scanning tunneling microscopy images show a surface with a 2×2 periodicity characterized by an high defect density. The corrugation of this surface is substantially higher than that of the clean surface. After annealing in vacuum at temperatures ranging from 600 to 800 K, a sharp 4×4 low-energy electron diffraction pattern can be observed. STM then reveals a superlattice of depressions, the remaining protrusions are slightly laterally displaced from their 2×2 positions. X-ray photoelectron diffraction intensities of the 4×4 phase show hardly any change for Pt $4f$, whereas Sn $3d$ azimuthal curves measured at higher polar angles are substantially modified after oxygen exposure. In order to understand the nature of the features observed in the STM images, the experimental XPD curves were compared with single and multiple scattering cluster calculations performed for various structural models. On the basis of these results we propose a model involving the reconstruction of the substrate surface.

DOI: 10.1103/PhysRevB.66.165416 PACS number(s): 81.65.Mq, 68.37.Ef, 61.14.Qp, 68.47.De

I. INTRODUCTION

The compositional and structural characterization of the phases formed upon oxygen exposure of Pt-Sn alloy surfaces is interesting from the point of view of the surface chemistry of this bimetallic system. Surfaces containing Pt and Sn are useful for hydrocarbon conversion as well as for the electrooxidation of methanol in fuel cells.[1–3] Tin oxide layers are expected to form by exposing Pt-Sn surfaces to O_2, considering the higher affinity toward oxygen of tin compared to platinum. Changes of the surface region composition occurring after oxygen exposure can modify substantially the functional properties of the alloy surface, in particular the chemical reactivity. Moreover, the study of the interaction of oxygen with Pt-Sn alloy surfaces is relevant considering the role of platinum in promoting the selectivity and sensitivity of gas sensors based on SnO_2.[4]

Early studies performed by means of surface sensitive techniques on polycrystalline Pt_3Sn surfaces reported an increase of tin concentration at the surface upon low-pressure exposures to oxygen.[5,6] Very recently, Batzill and co-workers investigated by means of Auger electron spectroscopy (AES), low-energy electron diffraction (LEED) and scanning tunneling microscopy (STM) the oxidation of Sn-Pt(111) surface alloys.[7–9] Such surface alloys were prepared by deposition of tin on Pt(111) and subsequent annealing. Several phases formed upon oxidation in various conditions of these surface alloys. These authors explained the LEED pattern and the STM images in terms of groups of tin and oxygen atoms (indicated as SnO ''pseudomolecules'') on the platinum surface. However, no information about the atomic structure of the protrusions observed in STM was reported.[8] In the present work we investigated by several surface sensitive techniques the phases formed on the $Pt_3Sn(111)$ surface after exposures at about 770 K to O_2 in the 10^{-6} mbar pressure range. Pt_3Sn is a substitutionally ordered alloy having the Cu_3Au type structure ($L1_2$ group). The clean $Pt_3Sn(111)$ surface has been thoroughly studied with a range of methods including LEED combined with low-energy ion scattering (LEIS),[10,11] LEED intensity analysis,[12] x-ray photoelectron diffraction (XPD),[13] spot profile analysis (SPA-) LEED combined with AES and LEIS,[14] Monte Carlo simulations using the ''macroscopic atom'' model,[15] and STM.[16] One of the aims of the present study was to obtain information about the reactivity of the $Pt_3Sn(111)$ surface toward oxygen. The evolution of the surface composition as a function of the oxygen exposure was followed by means of x-ray photoemission spectroscopy (XPS), AES, and LEIS.

The other purpose was to determine the atomic structure of the phases covering the substrate surface after low-pressure oxygen exposures. XPD measurements were performed on the surface phase formed after oxygen exposure in order to get information about the atomic structure of the features observed in the STM images.

II. EXPERIMENT

XPS/XPD, LEED, and LEIS measurements were performed in a ultrahigh-vacuum (UHV) system in Firenze with base pressures in the 5×10^{-10} mbar range. For XPS/XPD and LEIS a hemispherical electron/ion energy analyzer (HA100, Vacuum Science Workshop) was used. For LEED measurements the chamber is equipped with a reversed four-grid optics (Omicron). XPS/XPD experiments were performed with a nonmonochromatized Mg $K\alpha$ radiation source (1253.6 eV). The binding energy scale was calibrated using a silver standard and setting the Ag $3d_{5/2}$ binding energy (BE) to 368.3 eV.[17] The XPS spectra were recorded with a fixed pass energy of 44 eV, the fixed angle between x-ray source and analyzer was 55°, the semicone angle of acceptance of the analyzer was 4°. For XPS the spectra were measured at normal incidence. The sample was mounted on a manipulator that permits polar and azimuthal rotation. XPD curves were collected by monitoring the intensity of Pt $4f$ (1180.4 eV kinetic energy), Sn $3d_{5/2}$ (767.0 eV), Sn MNN Auger (427.8 eV), and (when appropriate) O $1s$ (722.0 eV) photoemission peaks. To estimate the background spectra at kinetic energies 5–10 eV higher than the peaks were taken. A Varian ion gun was used for sample cleaning and the LEIS measurements. All LEIS spectra were taken with 1000 eV He^+ ions, the analysis ion beam current density was of the order of 1×10^{-8} A/cm^2. The beam impinged with an angle of 45° off-normal onto the surface, the scattering angle was 135°.

The STM experiments were performed in an UHV system in Osnabrück using a Omicron STM I system operating at a base pressure below 5×10^{-11} mbar. All STM images have been measured in the constant current mode. AES spectra were acquired to check the cleanness of the surface, using an electron gun (Staib) and a 180° electrostatic analyzer (Physical electronics). A LEED system (of reversed four-grid Omicron type) was used to verify that after preparation the surface was in the same state to that achieved in Firenze. Sample cleaning and oxygen exposure were done in a separate preparation chamber. The $Pt_3Sn(111)$ sample was the same used in previous investigations.[16] The composition of the crystal (determined by means of an x-ray microprobe) was found to be 25 ± 0.5 at. % in Sn. The lattice parameter, measured by x-ray diffraction, was 4.00 Å, corresponding to a slight expansion with respect to pure platinum (3.92 Å).[12] In Firenze and in Osnabrück the clean $Pt_3Sn(111)$ single crystal was prepared following the procedure described in prior studies,[16] i.e., by several cycles of sputtering and thermal annealing to about 1000 K. For sputtering Ar^+ ions were used, in Firenze with an energy of 1000 eV, in Osnabrück with 600 eV. Thermocouples were used to monitor the sample temperature. The LEED patterns are indexed with respect to the lattice of the alloy containing only platinum. Hence the LEED pattern corresponding to the bulk truncated structure of $Pt_3Sn(111)$ is defined as 2×2.[12] Upon Ar-ion bombardment and annealing at circa 600 K, preferential sputtering of Sn atoms induced a reconstruction of the surface with $(\sqrt{3}\times\sqrt{3})R30°$ periodicity.[13] After annealing at 1000 K, the clean surface showed a sharp $p(2\times2)$ pattern with weak spots corresponding to the $(\sqrt{3}\times\sqrt{3})R30°$ reconstruction. For oxidation the 2×2 bulk-terminated sample was heated to 770 K and exposed to O_2 for typically several minutes. O_2 partial pressures of 1×10^{-6}–5×10^{-6} mbar were applied, typical doses were in the range of several thousand L (1 L corresponds to an exposure of 1 sec at a pressure of 1.33×10^{-6} mbar). In Osnabrück initial carbon contamination of the sample was easily removed by oxygen treatment, a procedure similar to oxygen exposure as described above (10 min O_2 at 5×10^{-6} mbar and 770 K) and subsequent heating to 1150 K for a further 5 min.

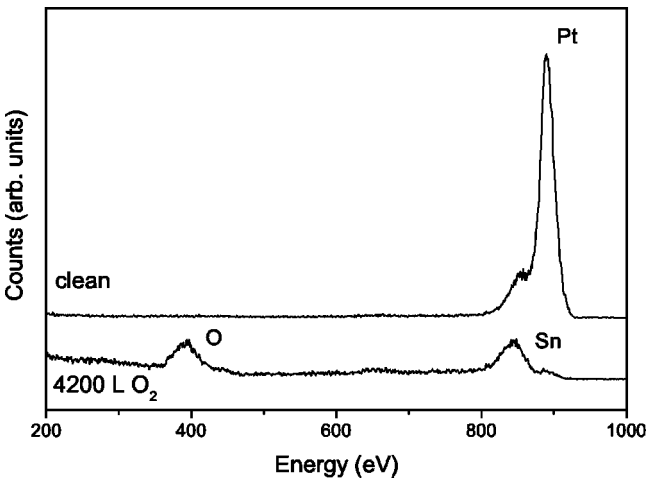

FIG. 1. LEIS spectra (1000 eV He^+) from the clean surface (top) and after exposing it to 9000 L O_2 (bottom) at 770 K. The scattering angle was 135°.

III. RESULTS AND DISCUSSION

XPS and LEIS were used to monitor the surface composition before and after oxidation. The superstructures observed by LEED are readily explained in view of STM images. XPD gives further insight into the surface structure.

A. XPS and LEIS

LEIS and XPS spectra were taken to follow the surface region composition upon oxygen exposure. As described above the oxidation experiments started from the clean 2×2 bulk-terminated $Pt_3Sn(111)$ surface. To study the influence of oxygen this surface was exposed to increasing O_2 doses. During all exposures the sample temperature was 770 K.

For analysis a linear background subtraction was applied to the LEIS data (see Fig. 1 for example curves) and the peak area measured. The elaboration of the XPS data (Fig. 2) consisted of smoothing, background subtraction (by means of

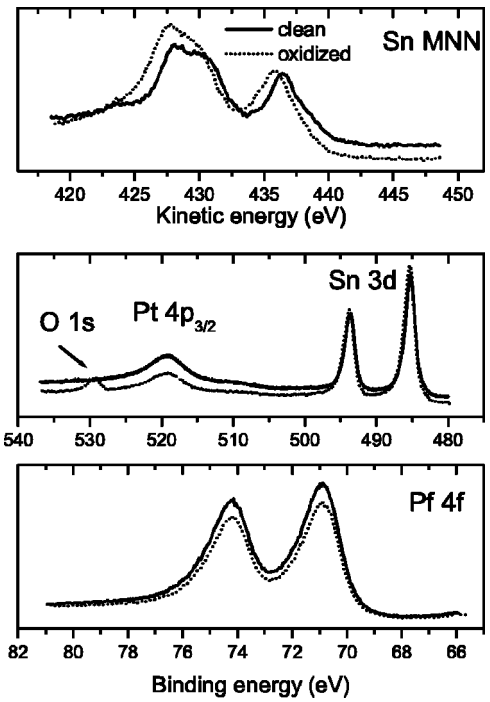

FIG. 2. XPS spectra of the clean surface (solid line) and after oxygen exposure (9000 L at 770 K) (dotted line) taken at polar angle 0° (normal emission) with Mg $K\alpha$ radiation (1253.6 eV).

the Shirley method) and peak area evaluation. In this way the data shown in Fig. 3 were obtained.

The O, Sn and Pt intensities determined from LEIS versus the O_2 exposure are shown in Fig. 3(a). With exposure the O concentration in the surface increases, Pt decreases. When the surface is saturated with oxygen, the platinum signal is barely detectable in the LEIS spectrum. The Sn signal increases for small oxygen doses but then drops to its initial value. As the total sum of the LEIS intensities decreases with exposure, this effect could be due to a geometric rearrangement of the scatterers. Since LEIS is virtually sensitive to the composition of the outermost layer only, these results indicate that the surface is completely covered by a tin-oxygen layer. The XPS curves of the Sn $3d_{5/2}$, O $1s$, and Pt $4f_{7/2}$ peak areas vs. the O_2 exposure indicate that the oxygen uptake process on the alloy surface reaches saturation after an exposure to about 5000 L [Fig. 3(b)]. The increase of the Sn signal and the decrease of the Pt signal is an indication that tin segregates at the surface upon oxygen exposure. This is consistent with prior studies of the oxidation of polycrystalline Pt_3Sn.[5,6,18,19] A comparison of the LEIS and XPS data in Fig. 3 shows that for Pt and O the respective spectra follow the same trends.

The Pt $4f$, Sn $3d$, O $1s$, and the Sn MNN Auger regions of the XPS spectra, collected for the clean surface and after an oxygen exposure of 9000 L, are shown in Fig. 2. For the clean surface, the Pt $4f_{7/2}$ and Sn $3d_{5/2}$ peaks are located at BE's of 70.9 and 485.3 eV, respectively. These values are very close to those measured for the pure platinum (71.0 eV) and pure tin (485.0 eV).[17] The BE's of both the Pt $4f_{7/2}$ and Sn $3d_{5/2}$ peaks do not change (within 0.1 eV) after oxygen exposure with respect to the values measured for the clean

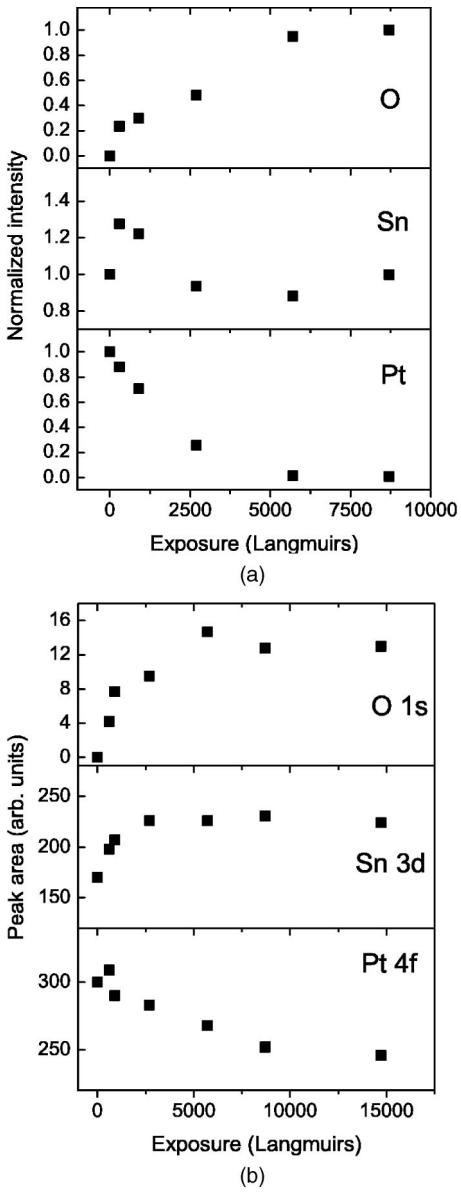

FIG. 3. LEIS (a) and XPS (b) intensities of the Pt, Sn, and O peaks as a function of the O_2 exposure. Pt and Sn LEIS intensities are normalized with respect to the clean surface values. The O LEIS signal is normalized to its maximum. The exposure was carried out at 770 K.

surface. The O $1s$ BE is 529.8 eV and does not change, within the experimental error bar, as a function of the oxygen exposure. No shoulder attributable to tin bound to oxygen is visible in the Sn $3d$ peaks. Only a slight broadening of the Sn $3d$ peaks on the high BE side can be observed. This can be explained with the fact that the BE of tin bound to oxygen is very close to that of Sn in the alloy. Indeed, the BE of the Sn $3d_{5/2}$ component, attributed to the ''quasimetallic'' state of tin determined for the oxidized Pt-Sn surface alloys, was found to be 485.3 eV.[20] In order to reveal changes in the chemical state of tin we considered the Auger parameter for the Sn MNN transition α, defined as the sum of the Sn $3d_{5/2}$ BE and the Sn $M_4N_{45}N_{45}$ kinetic energy.[21] The Auger parameter for the clean surface was found to be 921.7 eV, dif-

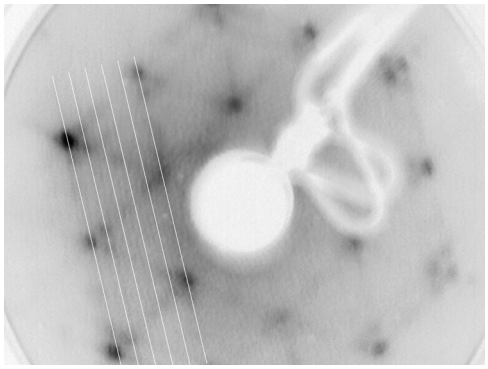

FIG. 4. LEED image (70.4 eV electron energy) after exposure to 6800 L O_2 at 770 K. The main spots located on 2×2 positions are interconnected by streaks. In these streaks additional spots occur at 1/5 of the 2×2 distances.

ferent from the value reported in the literature for pure tin (922.4 eV).[21] For the oxygen saturated surface the Auger parameter is 921.2 eV to be compared with the values reported for SnO (918.7 eV) and SnO_2 (919.2 eV).[21] The XPS data do not provide evidence of the formation of three-dimensional islands of tin oxide, either SnO or SnO_2. Hence the present results suggest the formation of a chemisorbed phase in which oxygen atoms are bound to tin atoms.

In the earlier studies of polycrystalline Pt_3Sn samples after exposure to O_2 or even air formation of a thicker tin oxide layer occurred that already exposed bulk properties.[6,18,19] There was a clear chemical shift for Sn $3d$, but none for Pt. It was reported that on the polycrystalline samples Sn mainly segregates through grain boundaries,[18] a mechanism not available on the $Pt_3Sn(111)$ single crystal. Instead, Sn segregates by lattice diffusion, a channel available only for higher temperatures than applied during the oxygen exposures.[14,15]

After this oxidation series, i.e. after a total O_2 dose of 9000 L, in the LEED a streaky 2×2 pattern with additional features on the connection lines of the main spots was observed. Upon annealing the sample to 620 K for 10 min a sharp 4×4 LEED pattern was observed (see Fig. 7 below with the according STM images). No changes could be detected in the XPS and LEIS spectra measured after the annealing in vacuum at 600–750 K. Only after prolonged annealing at 900–1000 K, a decrease of oxygen on the surface is observed.

B. Scanning tunneling microscopy

Typical STM images of the clean $Pt_3Sn(111)$ surface show 2×2 terraces with some residual $(\sqrt{3}\times\sqrt{3})R30°$ domains. In these images Pt atoms appear as protrusions whereas Sn atoms appear as holes due to the low local density of states of tin at the Fermi level.[16,22] A similar chemical contrast was also found on the $Pt_3Sn(001)$ and (110) surfaces.[23,24] To reproduce the preparation described above the cleaned sample was exposed to O_2 for 30 min at 770 K, i.e., 6800 L. Then LEED exhibited a streaky 2×2 pattern, as depicted in Fig. 4.

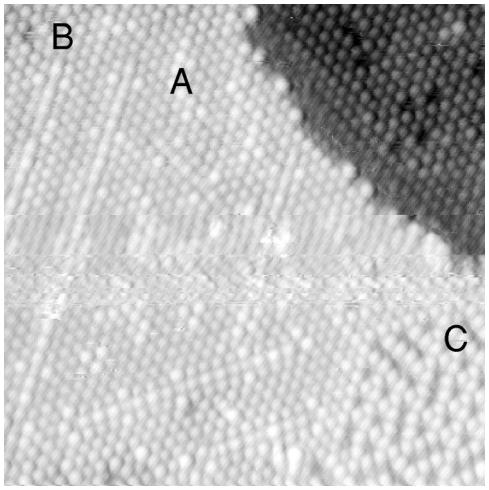

FIG. 5. STM image [$(200\ \text{Å})^2$, $U_T=-0.6$ V, $I_T=0.8$ nA)] after exposure to 6800 L O_2 at 770 K. The labels mark patches with (A) closed packed bump (B) defect lines, and (C) 4×4 depressions.

A STM image acquired after this preparation is shown in Fig. 5. The surface is mainly covered by a long range ordered mesh of protrusions with the same periodicity (5.6 Å) and orientation as the clean 2×2 surface. However, for the oxygen exposed surface only one clearly delimited protrusion appears in the surface unit cell. The corrugation of the protrusions is at typical tunnel parameters with 0.45 ± 0.10 Å significantly larger compared to 0.24 ± 0.10 Å of the clean 2×2 structure.

In the oxygen induced 2×2 phase several distinct defect features occur frequently. Point defects are quite common, typically arranged in locally ordered patches with depressions for every second protrusion in every second row, i.e., in a 4×4 superstructure. In addition sets of parallel defect lines about six rows apart are observed in the 2×2 structure. Along their direction the protrusions are displaced 1/2 lattice constant; here they are no longer close packed. At the ends of the lines small depressions are present. In some regions (in particular close to the steps at the upper side) structures quite different from the 2×2 structure are observed: groups of clusters more or less arranged in a hexagonal order (Fig. 6). These clusters consist of typically four protrusions of a size similar to that in the 2×2 structure, but in the clusters the arrangement of the protrusions is not uniform.

The nature of the protrusions observed in the STM topography of the tin-oxygen layer, and of the depressions is not obvious from the STM images. However, it is likely that they correspond to group of atoms not resolved in the images. In all STM images they act like clearly delimited entities. To simplify the further discussion we will refer to them as ''bumps'' and ''holes.''

The STM images of the structure obtained after heating to 700 K for 10 min of the oxidized sample reveal that the number of holes increased, the locally ordered 4×4 patches grew. During a sequence of experiments with increasing annealing temperatures in the range of 800–950 K the 4×4 LEED pattern became clearer, the long range order of the surface gradually improved. After annealing the oxidized

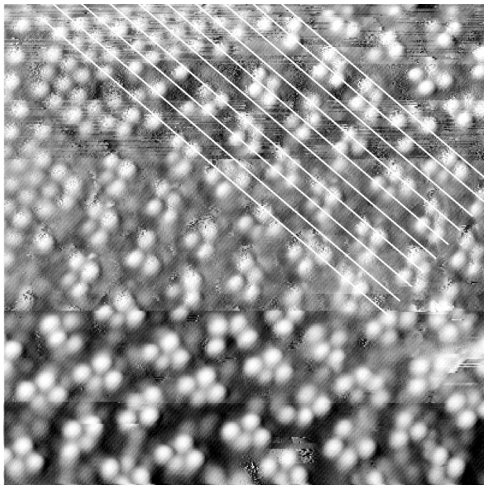

FIG. 6. STM image [$(120\ \text{Å})^2$, $U_T=-0.6$ V, $I_T=0.8$ nA] taken after the same preparation as Fig. 5. Clusters of typically four bumps occur which are separated about 1.5 lattice constants.

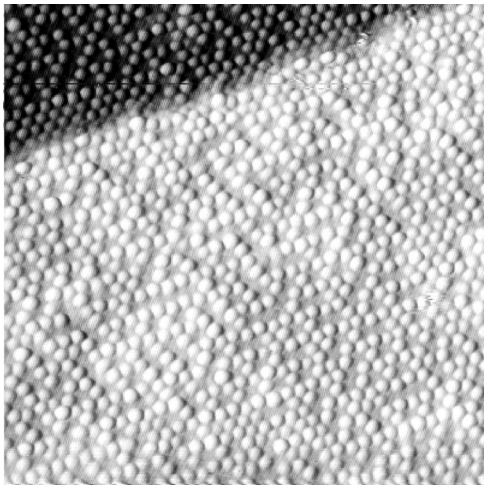

FIG. 8. STM image [$(200\ \text{Å})^2$, $U_T=+0.5$ V, $I_T=0.8$ nA] after exposure to 2300 L O_2 at 740 K. The surface structure is governed by the 4×4 structure.

sample at 950 K a clear 4×4 LEED pattern was obtained (as given in Fig. 7). STM images (Fig. 8) then show a long range 4×4 ordered surface. It was also possible to achieve long range ordered 4×4 regions by using lower O_2 doses of 2300 L for oxidation.

The 4×4 structure is the same as in the small defect patches in the 2×2 structure: every second bump in every second row is replaced by a hole. In some places the ideal hole mesh is disturbed by additional holes. STM yields a super-lattice constant of 11.4 ± 0.5 Å, i.e., twice that of the clean 2×2 surface. In view of this results the origin of the LEED superstructure is easily understood. As can be seen clearer in Fig. 9(a) the six bumps around a hole are alternately shifted toward and away from it. The bumps deviate approximately 0.5 ± 0.1 Å from the positions in a 2×2 mesh. A schematic model of the STM emphasizing the lateral displacements of the bumps is given in Fig. 9(b). Due to this displacements in the low-index directions the bumps are not exactly in line; the rows appear as ''zigzag'' lines. These zigzag lines look alike along all three low-index directions, which is only possible if the bumps are exactly shifted towards or away from the holes as indicated in Fig. 9(b). By the displacement the lateral distance of the bumps is slightly increased (about 0.08 Å). If the bumps corresponded to independent clusters this effect might be due to repulsive forces between them.

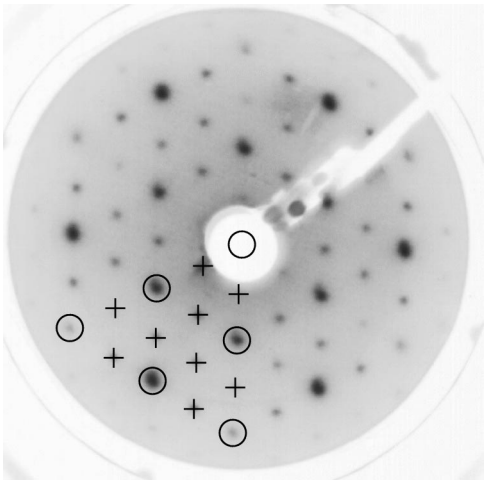

FIG. 7. LEED image (64.0 eV electron energy) after exposure to 6800 L O_2 at 770 K and subsequent annealing to 650 K. Spots already present in the 2×2 structure are indicated by circles, and the additional 4×4 spots by crosses.

In some images like Fig. 9(a) the bumps appear not perfectly spherical but slightly elliptic with their long axis oriented towards the hole, giving an impression of ''petals.'' As this effect is seen only for bumps adjacent to holes and then for all three axis directions at the same time, a double-tip effect can be ruled out. The corrugation of the bumps is 0.47 ± 0.13 Å, i.e., within the experimental uncertainty the same as in the 2×2 phase, whereas the holes are 1.08 ± 0.31 Å deep.

Variation of the gap voltage over a wide range of values (-4.0 to $+4.0$ V) sightly changed the corrugation, but the topography was otherwise unaffected. STM images could be obtained at low voltages like ±0.1 V. Thus the oxidized surface behaves metallic. The tin-oxygen layer is too thin to develop bulk properties of the semi-conductor tin oxide in agreement with the XPS results.

On the clean 2×2 surface the direction of step edges is basically determined by the local slope of the surface. After oxidation the steps tend to run along the low index directions forming hexagonal islands.

By heating the sample to 1050 K oxygen was completely desorbed from the surface. Afterward again a clean 2×2 surface was found, oxidation of $Pt_3Sn(111)$ can be revoked. In fact a preparation of oxygen exposure and desorption is quite similar to an oxygen treatment applied to remove carbon from the surface. To determine the registry between the substrate 2×2 and the oxygen related 4×4 phase, efforts were undertaken to image both phases in the same frame. In first attempts the oxidized sample was heated to 1000 K, i.e. almost the desorption temperature. Indeed in this way

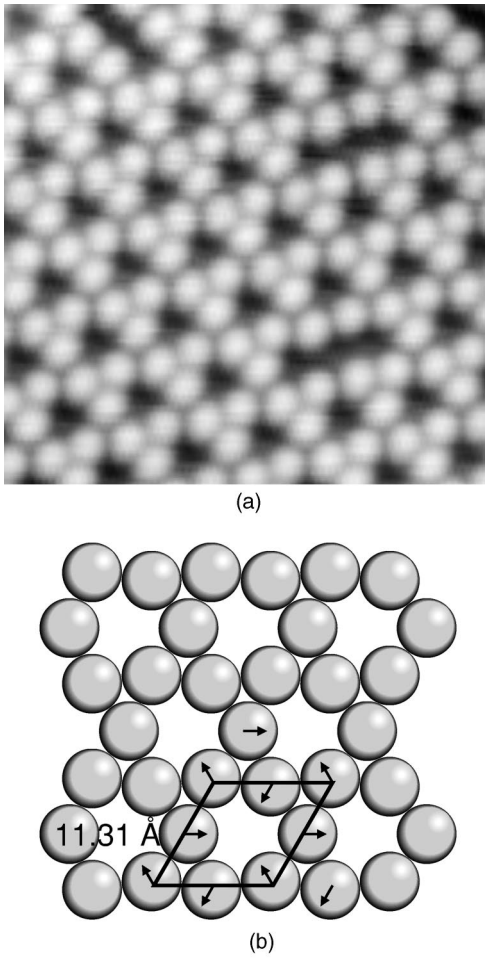

FIG. 9. The $Pt_3Sn(111)$ 4×4 structure: (a) small-scale STM image [$(68\ \text{Å})^2$, $U_T=+0.5$ V, $I_T=0.8$ nA], (b) schematic representation. (The balls represent one bump from the STM images each, in fact they might consist of more than one atom). A 4×4 unit cell is shown, the displacement directions of the bumps as observed by STM are indicated. To improve clearness the lateral displacements are enlarged.

oxygen was partially removed from the surface, but only terraces either completely 4×4 covered or completely clean were found in STM.

To overcome this problem the oxidized sample was sputtered for 10 s, corresponding to a ion dose of 4×10^{-5} C/cm^2. Afterwards according to AES oxygen was still present. STM showed the presence of many craters, exhibiting a depth of 2.0 ± 0.5 Å. After annealing at 900 K for 10 min flat terraces were found again. Larger uncovered 2×2 regions coexisted with domains of the oxygen related 4×4 phase (see Fig. 10). These images suggest that the protrusions in the O-Sn 4×4 phase are located at Sn positions of the substrate in the same layer. If the procedure to prepare 4×4 and clean surface coexisting patches produces antiphase domain boundaries, we should observe in-phase and antiphase domain boundaries. On the other hand, all the STM images obtained after the reported treatment show that the protrusions of the 4×4 phase are located at the position of Sn atoms of the clean surface.

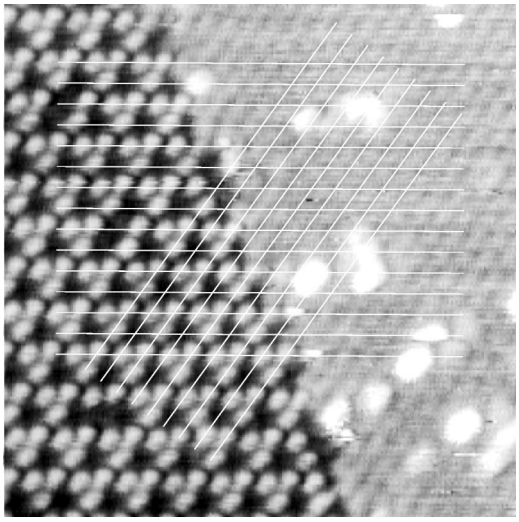

FIG. 10. STM image [$(116\ \text{Å})^2$, $U_T=+0.8$ V, $I_T=0.6$ nA] after sputtering a 4×4 substrate for 8 sec and annealing at 900 K for 10 min. The registry between the oxygen 4×4 phase and the 2×2 substrate is indicated by lines.

In recent studies Batzill and co-workers worked on the oxidation of Sn-Pt(111) surface alloys by exposure to NO_2.[7–9] After complete oxidation they found a highly ordered superlattice of SnO_x islands on the Pt(111) substrate. The corresponding LEED showed a sharp 5×5 pattern. These islands are in many ways similar to the clusters found on Pt_3Sn after high oxygen doses (see Fig. 6). In larger scale images they look alike, the typical arrangement (distances etc.) appears to be identical. The STM topography of the islands as found on the oxygen-Sn-Pt(111) did not reveal any substructure, while on $Pt_3Sn(111)$ resolution within the islands was obtained, showing that they consist of typical four not too well ordered bumps. Note that in the streaky 2×2 LEED pattern additional spots occurred at one fifth of the 2×2 distances (see Fig. 4), i.e., on 10×10 positions. They can be explained by the formation of a 5×5 island structure as described in Refs. 7–9 on the Pt_3Sn 2×2 substrate.

After annealing to 800–1000 K Batzill and co-workers observed a 4×4 LEED pattern. The STM images given in Ref. 8 show a structure compatible with the 4×4 pattern described above, but with a not as pronounced long range order. No lateral displacement of the bumps was observed on the surface alloy. Otherwise the authors gave a model for the 4×4 structure similar to that given in Fig. 9(b). They interpreted the protrusions as Sn_xO_y ''molecules'' populating Pt sites on a 2×2 Sn-Pt(111) surface alloy substrate.

In the studies of oxidized Sn-Pt(111) surface alloys a general behavior similar to that of the alloy surface $Pt_3Sn(111)$ was found. Nevertheless the STM images of the alloy surface included details not present in the surface alloy images (e.g., the inner structure of the SnO_x nanodots and the displacement of the bumps). The observed minor differences may be due to different preparation procedures of the O-Sn layers. The presence of tin in the substrate (in the case of the alloy surface) is also expected to influence the thermal stability of the Sn-O layer. Moreover, the sligthly different lattice param-

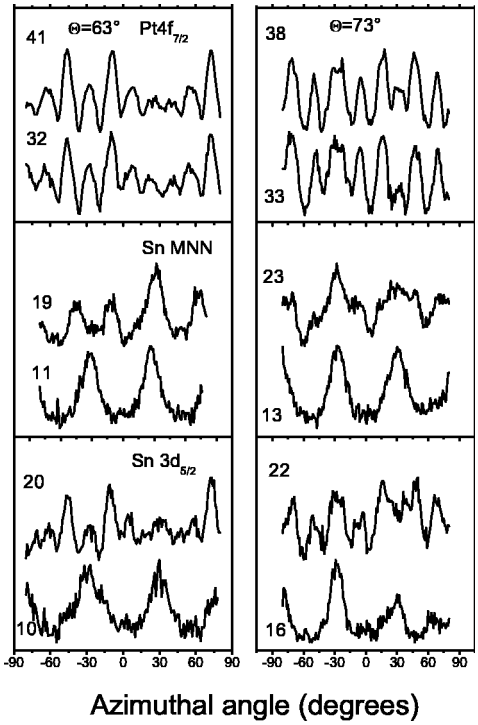

FIG. 11. Comparison of the Pt $4f_{7/2}$, Sn MNN, and Sn $3d_{5/2}$ azimuthal XPD curves measured for the clean surface and for the 4×4 superstructure obtained after an oxygen exposure of 9000 L (pressure: 5×10^{-6} mbar, sample temperature: 770 K) and annealing at 600 K for 10 min. Left column: azimuthal XPD curves measured at a polar angle of 63°. Right column: azimuthal XPD curves measured at a polar angle of 73°. The polar angles are defined with respect to the normal to the surface. In each panel the top curve corresponds to the clean surface. The maximum value of the modulation amplitude, $(I_{max}-I_{min})/I_{max}[\%]$, is reported for each curve.

eters of Pt_3Sn and Pt(111) may play an important role in stabilizing the various superstructures.

Sn in deeper layers or segregated from the bulk (present only in the bulk alloy) might influence the surface local density of states (LDOS). Simulations of the LDOS at both surfaces would be helpful to decide what reason prevails.

C. X-ray photoelectron diffraction

As shown by LEED and STM, the 2×2 phase formed by oxygen exposure at 770 K without further annealing is characterized by an higher concentration of defects and disorder with respect to the 4×4 superstructure. Hence, to obtain information about the nature of the protrusions observed in the STM pictures, only the latter phase was investigated in detail by means of XPD. Pt $4f_{7/2}$, Sn MNN and Sn $3d_{5/2}$ azimuthal XPD curves measured for the clean surface and for the 4×4 superstructure obtained after oxygen exposure are shown in Fig. 11. Pt $4f_{7/2}$ and Sn $3d_{5/2}$ full angular scans taken from the clean 2×2 surface (Fig. 12) show patterns typical for a fcc (111) surface, exhibiting a threefold symmetry. The kinetic energy of the emitted electrons is in both cases sufficiently high to let the patterns be governed by forward scattering enhancement.[25] Pt $4f_{7/2}$ XPD curves measured for the clean surface and for the 4×4 phase are virtually the same. On the other hand, Sn $3d_{5/2}$ and Sn MMN XPD curves show significant variations after oxygen exposure but only at higher polar emission angles (see Fig. 12).

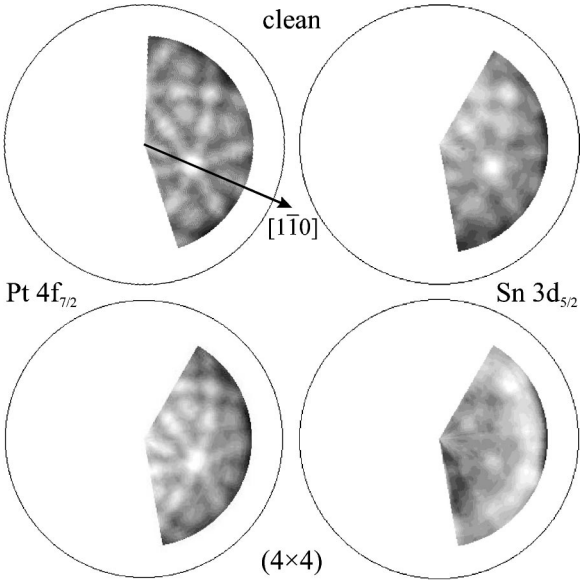

FIG. 12. Stereographic representation of Pt $4f_{7/2}$ (left) and Sn $3d_{5/2}$ XPD patterns (right) measured for the clean $Pt_3Sn(111)$ surface (top) and for the $Pt_3Sn(111)$ 4×4 phase (bottom). The strongest diffraction features at a polar angle of 35° corresponds to the $[1\bar{1}0]$ azimuthal direction. The intensities are represented on a gray-level scale. They were measured for polar angles θ between 0° and 70°.

The O $1s$ XPD curves do not show any intensity modulation within the noise level, that is the amplitude of the intensity modulations is below 5%. The rather high noise level is due to the fact that the relatively weak oxygen O $1s$ signal is located on the tail of the Pt $3p_{3/2}$ peak. Such inelastic tail is modulated as a function of the emission angle like the Pt $3p_{3/2}$ peak. The XPD results are consistent with the formation of a tin-oxygen phase which is a few atomic layers thick. Moreover, the lack of intensity modulations of the O $1s$ XPD curves (due to forward scattering along interatomic directions) suggests that there are no scattering centers above the oxygen atoms. The low thickness of the oxygen phase compared to the depth probed by the Pt $4f_{7/2}$ photoelectrons (having a relatively high kinetic energy) can partly explain why the Pt $4f$ XPD curves do not change after oxygen exposure. However, since the depth probed by the Pt $4f$ and Sn $3d$ photoelectrons is not so different, other effects should play a role in determining the different behavior of the Sn and Pt XPD curves after oxygen exposure (see below).

In the Sn $3d_{5/2}$ XPD pattern the most intense features which appear after oxygen exposure are located a polar angle of about 60°. At this polar angle diffraction features having nearly the same intensity are observed every 60° in the azimuthal curves. If Sn atoms in the overlayer give a sixfold symmetrical pattern, this contribution summed with that one from the bulk can explain the observed symmetry. This in-

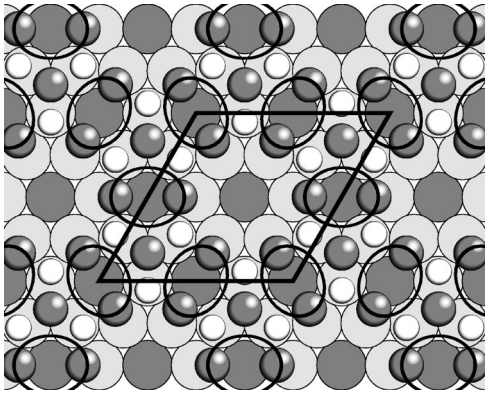

FIG. 13. Schematic model of the 4×4 phase. Simple light gray circles: platinum atoms in the substrate, simple dark gray circles: tin atoms in the substrate. Dark gray balls: tin atoms in the overlayer. White balls: oxygen atoms. In this model two Sn atoms in the overlayer together with a adjacent substrate Sn atom appear as one protrusion in the STM (indicated by the ellipses). A unit cell corresponding to that in Fig. 9(b) is shown.

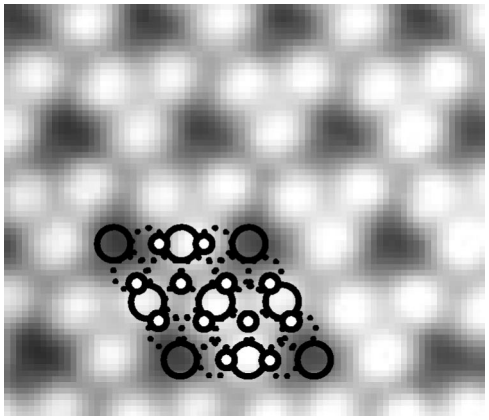

FIG. 14. Structural model for the 4×4 phase proposed on the basis of the XPD data superimposed on the STM image. Small circles: Sn in the overlayer. Large circles: Sn atoms (solid line) and Pt atoms (dashed line) in the topmost layer of the alloy. Oxygen atoms are not shown.

terpretation also implies that the contribution to the XPD oscillations from tin atoms in the oxygen phase is maximal around a polar angle of 60°.

XPD curves measured for the 4×4 phase are very similar to those collected for the surface showing the streaky 2×2 surface (that is after oxygen exposure without annealing in vacuum). This suggests that the local structure of Sn is the same in the two surfaces.

To get further information about the atomic structure of the 4×4 phase, we performed calculations of the diffraction curves considering various structural models. We used single scattering cluster (SSC) calculations[25] in a first screening of the structural models to reduce the computational effort. The structure of the crystal was described as a cluster whose size is determined by a maximum length of the path between the emitter and the scatterers. In the present calculations this length was set to 12 Å. Larger values of this parameter did not produce any significant variation of the calculated XPD curves. The O, Sn, and Pt phase shifts were calculated using the Van Hove and Barbieri program package.[26]

Multiple scattering calculations were carried out using the MSCD (multiple scattering calculation of diffraction) package developed by Chen and Van Hove.[27] Structural models based on oxygen atoms adsorbed on a unreconstructed surface could be ruled out since the Sn XPD intensities calculated for these structures differ only slightly from those calculated for the clean surface (mainly a variation of the relative intensities of some features in the curves). On the basis of the XPD patterns, we propose a possible model involving a reconstruction of the alloy surface. In the model, shown in Fig. 13, Sn atoms have a hexagonal arrangment. The positions of the atoms were chosen in such a way to have the forward scattering maxima in the azimuthal directions observed in the Sn $3d$ XPD pattern. The protrusions in the STM images would correspond to groups of tin atoms, each consisting of two tin atoms in the overlayer located adjacent to a substrate tin atom sitting in the center between them (see Fig. 14).

The arrangement of Sn atoms is similar that of Sn atoms in the (101) plane of SnO.[28,29] In particular, one side of the unit cell of Sn0(101) is equal to the Sn-Sn nearest-neighbor distance in the proposed model (3.77 Å). This would produce a 4×4 coincidence cell with the periodicity of the substrate. In the proposed model Sn atoms which would occupy on-top positions (at the corner of the unit cell) are missing. The missing of these atoms would produce the holes observed in STM. The composition of this overlayer is Sn_8O_6. The results of the SSC calculations performed for this model are shown in Fig. 15. The SSC calculations indicate that the major contribution to the additional features in the XPD curves measured for the 4×4 phase are due to photoelectrons emitted by Sn atoms in the overlayer and scattered by oxygen atoms. The curves shown here were calculated for the parameters giving the best fit with the experimental data, estimated from the visual comparison and the *R*-factor

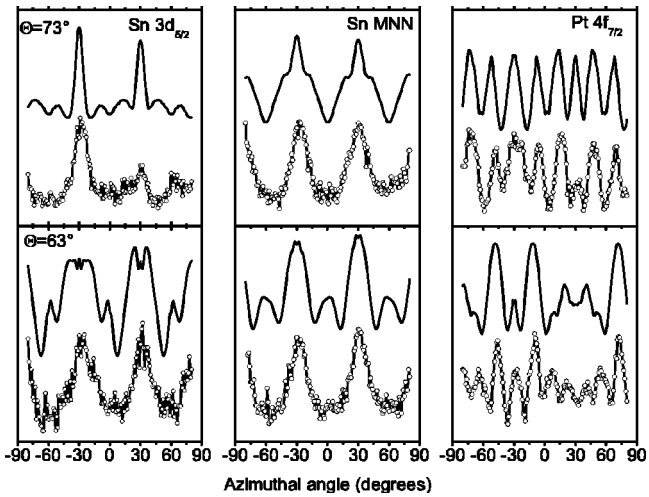

FIG. 15. Comparison of experimental Sn $3d_{5/2}$, Sn MNN, and Pt $4f_{7/2}$ azimuthal XPD curves (circles and solid line) with the SSC calculations (solid line) performed for the model depicted in Fig. 13.

analysis.[27] The best agreement between experimental and calculated data was obtained for a O-Sn interlayer distance of 1.0 ± 0.1 Å. In this model the O-Sn bond length is 2.4 Å. The O-Sn bond length is longer than the O-Sn nearest-neighbor distances in SnO (2.21 Å) and SnO_2 (2.06 Å).[28,29] It should be noted that the sensitivity of the curves to the vertical distance of the oxygen atoms with respect to the tin atoms in the overlayer is rather low. The level of agreement of the XPD curves calculated for this model is only moderate, since some features of the experimental XPD curves are not reproduced in a satisfactory way. These calculations show that the Pt $4f$ XPD patterns are not significantly influenced by the formation of the overlayer Sn-O, in agreement with the experimental findings. This fact can be explained considering that the Pt atoms are arranged in various local structures with respect to the Sn-O overlayer. Hence the scattering from the overlayer is averaged over these local structures while the contribution from substrate atoms is not substantially affected. Conversely, all Sn atoms ''see'' the oxygen atoms in the same way. Hence we can conclude that the proposed model is able to explain many of the experimental findings. However, the model cannot reproduce the lateral shift of the bumps observed in STM. In addition it cannot explain the dense Sn-O 2×2 structure for which STM topographs show four equivalent protrusions per 4×4 unit cell. Albeit not displaced, these protrusions are otherwise similar to that in the 4×4 structure.

Since the Sn 3d XPD has a contribution from tin atoms in the substrate an accurate description of this component could be crucial in the calculations. Hence we performed additional multiple scattering (MS) calculations of the XPD intensity of the proposed structural model. The MS method which properly takes into account defocusing effects should provide a better description of the contribution of the bulk to the XPD intensities. The calculations were performed only for the Sn $3d_{5/2}$ XPD curves. Calculations of the XPD curves obtained monitoring the intensity Sn *MNN* Auger peak could not be performed because of the difficulties in describing the angular momentum of the outgoing Auger electrons. The MS simulations could not be performed for the Pt $4f$ XPD curves because of the too large number of emitters. The MS calculations of the Sn $3d$ XPD curves substantially reproduce the SSC intensities. Hence we may conclude that in the present case single scattering calculations provide a reliable description of the experimental data. We also considered a possible variation of the Sn concentration in the first substrate layer. In the MS calculations we simulated a Sn depletion by removing Sn atoms in the topmost layer of the substrate. In the SSC calculations the composition of the substrate surface could be varied continuously.[30] The results of these model calculations do not provide any evidence for depletion of tin in the surface region of the alloy since the agreement between calculated and experimental XPD curves does not improve upon varying the concentration of Sn in the surface region of the alloy.

IV. CONCLUSIONS

Oxygen adsorption on the $Pt_3Sn(111)$ surface has been investigated using XPS, LEIS, STM, LEED, AES, and XPD. Oxygen adsorption on $Pt_3Sn(111)$ at 770 K and at a pressure of circa 5×10^{-6} mbar is a self-limiting process leading to the saturation of the surface with a layer containing oxygen and tin. After exposure to 9000 L O_2 under these conditions streaky 2×2 LEED patterns are found. STM showed a 2×2 lattice of highly corrugated protrusions with various defect structures. Upon annealing at temperatures ranging from 600 to 800 K, a sharp 4×4 LEED pattern is observed. STM revealed that the 4×4 structure is determined by a long range ordered supermesh of depressions with twice the lattice constant of the 2×2 structure. The protrusions are alternatingly displaced laterally towards and away from the depressions. It is unclear which species are imaged as protrusions in the STM topography. Desorption experiments allowed one to assign the holes in the STM topography to missing atoms or agglomerates containing oxygen. A similar 4×4 structure was found for the oxidation under various conditions of Pt-Sn surface alloys prepared by annealing of tin deposited on Pt(111). By means of XPD we obtained information about the atomic structure of the 4×4 phase. The XPD results suggest that at saturation coverage the substrate surface is covered by a two-dimensional phase. The Pt XPD curves are not affected by oxygen exposure, whereas the Sn $3d$ and Sn *MNN* XPD intensities at higher polar angles are significantly modified upon the formation of the 4×4 phase. The most intense features which appear after oxygen exposure in the Sn $3d_{5/2}$ XPD pattern are located a polar angle of about 60°. The Sn $3d$ XPD pattern can be explained if Sn atoms in the overlayer give a sixfold symmetrical pattern. This contribution summed with that one from the bulk can explain the observed symmetry. On the basis of these results we proposed a structural model in which Sn atoms are arranged in a similar way as in the (101) plane of SnO. This model is consistent with 4×4 STM images, assuming that the bumps seen by STM correspond to groups of tin atoms, each consisting of two overlayer Sn atoms and one Sn substrate atom between them. It is in agreement with the registry of the O-Sn overlayer determined by STM, i.e., the bumps are located on top of Sn atoms in the substrate surface. Although the level of agreement is only moderate, the XPD curves calculated for this model reproduce the main features of the experimental data. But as the 2×2 structure cannot be explained easily, the given model is only tentative. The atomic structure of the 4×4 phase cannot be considered solved, but nonetheless the XPD results allowed us to reduce to the number of possible structural models.

ACKNOWLEDGMENTS

This work was supported by the Deutsche Forschungsgemeinschaft (DFG), the Stichting voor Fundamenteel Onderzoek der Materie (FOM), the European Science Foundation (ESF) within the ALEnet project, and the MURST under the program ''Crescita, struttura e reattività di superfici di materiali e di film superficiali'' COFIN2000.

*Corresponding author. Electronic address: mhoheise@sci.kun.nl

[1] F. M. Dautzenberg, J. N. Helle, P. Biloen, and W. M. H. Sachtler, J. Catal. **63**, 119 (1980).
[2] K. Wang, H. A. Gasteiger, N. M. Markovic, and P. N. Ross Jr., Electrochim. Acta **41**, 2587 (1996).
[3] C. Panja, N. Saliba, and B. E. Koel, Surf. Sci. **395**, 248 (1998).
[4] W. Goepel and K. D. Schierbaum, Sens. Actuators B **26–27**, 1 (1995).
[5] G. B. Hoflund, D. A. Ashbury, P. Kirszensztejn, and H. A. Laitinen, Surf. Sci. **161**, L583 (1985).
[6] D. A. Ashbury and G. B. Hoflund, Surf. Sci. **199**, 552 (1988).
[7] M. Batzill, D. E. Beck, and B. E. Koel, Appl. Phys. Lett. **78**, 2766 (2001).
[8] M. Batzill, D. E. Beck, D. Jerdev, and B. E. Koel, J. Vac. Sci. Technol. A **19**, 1953 (2001).
[9] M. Batzill, D. E. Beck, and B. E. Koel, Phys. Rev. B **64**, 245402 (2001).
[10] A. N. Haner, P. N. Ross, and U. Bardi, Surf. Sci. **249**, 15 (1991).
[11] A. Haner, P. Ross, and U. Bardi, Catal. Lett. **8**, 1 (1991).
[12] A. Atrei, U. Bardi, G. Rovida, M. Torrini, E. Zanazzi, and P. N. Ross, Phys. Rev. B **46**, 1649 (1992).
[13] A. Atrei, U. Bardi, M. Torrini, E. Zanazzi, G. Rovida, H. Kasamura, and M. Kudo, J. Phys.: Condens. Matter **5**, L207 (1993).
[14] W. C. A. N. Ceelen, A. W. Denier van der Gon, M. A. Reijme, H. H. Brongersma, I. Spolveri, A. Atrei, and U. Bardi, Surf. Sci. **406**, 264 (1998).
[15] C. Creemers and S. Helfensteyn, Appl. Surf. Sci. **167**, 216 (2000).
[16] J. Kuntze, S. Speller, W. Heiland, A. Atrei, I. Spolveri, and U. Bardi, Phys. Rev. B **58**, R16 005 (1998).
[17] *Handbook of X-Ray Photoelectron Spectroscopy*, edited by J. Chastain (Perkin-Elmer Corporation, Physical Electronics Division, 6509 Flying Cloud Drive, Eden Prairie, Minnesota 55344, 1992).
[18] G. B. Hoflund, D. A. Ashbury, P. Kirszensztejn, and H. A. Laitinen, Surf. Interface Anal. **9**, 169 (1986).
[19] G. B. Hoflund and D. A. Ashbury, Langmuir **2**, 695 (1986).
[20] D. I. Jerdev and B. E. Koel, Surf. Sci. **492**, 106 (2001).
[21] D. Briggs and M. P. Seah, eds., *Practical Surface Analysis*, 2nd ed. (Wiley, Chichester, 1990).
[22] Š. Pick, Surf. Sci. **436**, 220 (1999).
[23] M. Hoheisel, J. Kuntze, S. Speller, A. Postnikov, W. Heiland, I. Spolveri, and U. Bardi, Phys. Rev. B **60**, 2033 (1999).
[24] M. Hoheisel, S. Speller, J. Kuntze, A. Atrei, U. Bardi, and W. Heiland, Phys. Rev. B **63**, 245403 (2001).
[25] C. S. Fadley, in *Synchrotron Radiation Research: Advances in Surface and Interface Science*, edited by R. Z. Bachrach (Plenum Press, New York, 1992), Chap. 11.
[26] M. A. Van Hove and A. Barbieri, *Phase Shift Package* (private communication) URL http://electron.lbl.gov/software
[27] Y. Chen and M. A. Van Hove, URL http://electron.lbl.gov/mscdpack/
[28] A. F. Wells, *Structural Inorganic Chemistry* (Clarendon, Oxford, 1985).
[29] R. W. G. Wychoff, *Crystal Structures* (Wiley, New York, 1964).
[30] M. Galeotti, A. Atrei, U. Bardi, G. Rovida, and M. Torrini, Surf. Sci. **313**, 349 (1994).